



# Compact single-etched sub-wavelength grating couplers for O-band application

**YUN WANG,\* LUHUA XU, AMAR KUMAR, YANNICK D'MELLO, DAVID PATEL, ZHENPING XING, RUI LI, MD GHULAM SABER, ESLAM EL-FIKY, AND DAVID V. PLANT**

*Department of Electrical and Computer Engineering, McGill University, Montreal, Quebec, Canada  
\*yun.wang5@mcgill.ca*

**Abstract:** We demonstrate two single-etched sub-wavelength grating coupler (SWGC) designs for O-band application, one targeting at high coupling efficiency and the other targeting at broad operating bandwidth. The high-efficiency SWGC has a measured peak coupling efficiency of  $-3.8$  dB and a 3-dB bandwidth of 40 nm, and the broadband SWGC has a measured peak coupling efficiency of  $-4.3$  dB and a 3-dB bandwidth of 71 nm. Focusing gratings have been used in our SWGCs to reduce the design footprints and the dimensions of our SWGCs are smaller than  $45\text{ }\mu\text{m} \times 24\text{ }\mu\text{m}$ . The back reflections of our SWGCs are suppressed to be below  $-15$  dB over the wavelength range from 1260 nm to 1360 nm.

© 2017 Optical Society of America under the terms of the [OSA Open Access Publishing Agreement](#)

**OCIS codes:** (050.6624) Subwavelength structures; (050.1950) Diffraction gratings.

## References and links

1. S. J. McNab, N. Moll, and Y. A. Vlasov, "Ultra-low loss photonic integrated circuit with membrane-type photonic crystal waveguides," *Opt. Express* **11**(22), 2927-2939 (2003).
2. P. Cheben, J. H. Schmid, S. Wang, D. X. Xu, M. Vachon, S. Janz, J. Lapointe, Y. Painchaud, and M.-J. Picard, "Broadband polarization independent nanophotonic coupler for silicon waveguides with ultra-high efficiency," *Opt. Express* **23**(17), 22553-22563 (2015).
3. A. Mekis, S. Gloeckner, G. Masini, A. Narasimha, T. Pinguet, S. Sahni, and P. De Dobbelaere, "A grating-coupler-enabled CMOS photonics platform," *IEEE J. Sel. Top. Quantum Electron.* **17**(3), 597-608 (2011).
4. G. Roelkens, D. Vermeulen, S. Selvaraja, R. Halir, W. Bogaerts, and D. Van Thourhout, "Grating-based optical fiber interfaces for silicon-on-insulator photonic integrated circuits," *IEEE J. Sel. Top. Quantum Electron.* **17**(3), 571-580 (2011).
5. A. Novack, Y. Liu, R. Ding, M. Gould, T. Baehr-Jones, Q. Li, Y. Yang, Y. Ma, Y. Zhang, K. Padmaraju, A. Lim, G. Lo, and M. Hochberg, "A 30 GHz silicon photonic platform," in *Proceedings of IEEE 10th International Conference on Group IV Photonics* (2013), pp. 7-8.
6. W. S. Zaoui, A. Kunze, W. Vogel, M. Berroth, J. Butschke, F. Letzkus, and J. Burghartz, "Bridging the gap between optical fibers and silicon photonic integrated circuits," *Opt. Express* **22**(2), 1277-1286 (2014).
7. W. D. Sacher, Y. Huang, L. Ding, B. J. Taylor, H. Jayatilleka, G.-Q. Lo, and J. K. Poon, "Wide bandwidth and high coupling efficiency  $\text{Si}_3\text{N}_4$ -on-SOI dual-level grating coupler," *Opt. Express* **22**(9), 10938-10947 (2014).
8. L. Vivien, D. Pascal, S. Lardenois, D. Marris-Morini, E. Cassan, F. Grillot, S. Laval, J.-M. Fédié, and L. El Melhaoui, "Light injection in SOI microwaveguides using high-efficiency grating couplers," *J. Lightwave Technol.* **24**(10), 3810-3815 (2006).
9. N. Na, H. Frish, I.-W. Hsieh, O. Harel, R. George, A. Barkai, and H. Rong, "Efficient broadband silicon-on-insulator grating coupler with low backreflection," *Opt. Lett.* **36**(11), 2101-2103 (2011).
10. R. Shi, H. Guan, A. Novack, M. Streshinsky, A. E-J. Lim, G.-Q. Lo, T. B.-Jones, and M. Hochberg, "High-efficiency grating couplers near 1310 nm fabricated by 248-nm DUV lithography," *IEEE Photonics Technol. Lett.* **26**(15), 1569-1572 (2014).
11. M. T. Wade, F. Pavanello, R. Kumar, C. M. Gentry, A. Atabaki, R. Ram, V. Stojanovic, and M. A. Popovic, 2015. "75% efficient wide bandwidth grating couplers in a 45 nm microelectronics CMOS process," in *IEEE Optical Interconnects Conference* (2015), pp. 46-47.
12. D. Benedikovic, C. Alonso-Ramos, P. Cheben, J. H. Schmid, S. Wang, R. Halir, A. Ortega-Moñux, D.-X. Xu, L. Vivien, J. Lapointe, S. Janz, and M. Dado, "Single-etch subwavelength engineered fiber-chip grating couplers for  $1.3\text{ }\mu\text{m}$  datacom wavelength band," *Opt. Express* **24**(12), 12893-12904 (2016).
13. X. Chen, D. J. Thomson, L. Crugdinton, A. Z. Khokhar, and G. T. Reed, "Dual-etch apodised grating couplers for efficient fibre-chip coupling near 1310 nm wavelength," *Opt. Express* **25**(15), 17864-17871 (2017).

14. S. Wang, Y. Hong, Y. Zhu, J. Chen, S. Gao, X. Cai, Y. Shi, and L. Liu, "Compact high-efficiency perfectly-vertical grating coupler on silicon at O-band," *Opt. Express* **25**(18), 22032–22037 (2017).
15. R. Halir, P. J. Bock, P. Cheben, A. Ortega-Moñux, C. Alonso-Ramos, J. H. Schmid, J. Lapointe, D.-X. Xu, J. G. Wangüemert-Pérez, I. Molina-Fernández, and S. Janz, "Waveguide sub-wavelength structures: a review of principles and applications," *Laser & Photonics Rev.* **9**(1), 25–49 (2015).
16. P. Cheben, P. J. Bock, J. H. Schmid, J. Lapointe, S. Janz, D.-X. Xu, A. Densmore, A. Delâge, B. Lamontagne, and T. J. Hall, "Refractive index engineering with subwavelength gratings for efficient microphotonic couplers and planar waveguide multiplexers," *Opt. Lett.* **35**(15), 2526–2528 (2010).
17. P. J. Bock, P. Cheben, J. H. Schmid, J. Lapointe, A. Delâge, D.-X. Xu, S. Janz, A. Densmore, and T. J. Hall, "Subwavelength grating crossings for silicon wire waveguides," *Opt. Express* **18**(15), 16146–16155 (2010).
18. R. Halir, P. Cheben, J. M. Luque-González, J. D. Sarmiento-Merenguel, J. H. Schmid, G. Wangüemert-Pérez, D.-X. Xu, S. Wang, A. Ortega-Moñux, and I. Molina-Fernández, "Ultra-broadband nanophotonic beamsplitter using an anisotropic sub-wavelength metamaterial," *Laser Photonics Rev.* **10**(6), 1039–1046 (2016).
19. J. Flueckiger, S. Schmidt, V. Donzella, A. Sherwali, D. M. Ratner, L. Chrostowski, and K. C. Cheung, "Sub-wavelength grating for enhanced ring resonator biosensor," *Opt. Express* **24**(14), 15672–15686 (2016).
20. Y. Wang, X. Wang, J. Flueckiger, H. Yun, W. Shi, R. Bojko, N. A. Jaeger, and L. Chrostowski, "Focusing sub-wavelength grating couplers with low back reflections for rapid prototyping of silicon photonic circuits," *Opt. Express* **22**(17), 20652–20662 (2014).
21. Y. Wang, H. Yun, Z. Lu, R. Bojko, W. Shi, X. Wang, J. Flueckiger, F. Zhang, M. Caverley, N. A. Jaeger and Lukas Chrostowski, "Apodized focusing fully etched subwavelength grating couplers," *IEEE Photonics J.* **7**(3), 1–10 (2015).
22. Y. Wang, W. Shi, X. Wang, Z. Lu, M. Caverley, R. Bojko, L. Chrostowski, and N. A. Jaeger, "Design of broadband subwavelength grating couplers with low back reflection," *Opt. Lett.* **40**(20), 4647–4650 (2015).
23. R. Halir, P. Cheben, J. Schmid, R. Ma, D. Bedard, S. Janz, D.-X. Xu, A. Densmore, J. Lapointe, and I. Molina-Fernández, "Continuously apodized fiber-to-chip surface grating coupler with refractive index engineered subwavelength structure," *Opt. Lett.* **35**(19), 3243–3245 (2010).
24. Z. Cheng, X. Chen, C. Y. Wong, K. Xu, and H. K. Tsang, "Apodized focusing subwavelength grating couplers for suspended membrane waveguides," *Appl. Phys. Lett.* **101**(10), 101104 (2012).
25. X. Xu, H. Subbaraman, J. Covey, D. Kwong, A. Hosseini, and R. T. Chen, "Colorless grating couplers realized by interleaving dispersion engineered subwavelength structures," *Opt. Lett.* **38**(18), 3588–3591 (2013).
26. Q. Zhong, V. Veerasubramanian, Y. Wang, W. Shi, D. Patel, S. Ghosh, A. Samani, L. Chrostowski, R. Bojko, and D. V. Plant, "Focusing-curved subwavelength grating couplers for ultra-broadband silicon photonics optical interfaces," *Opt. Express* **22**(15), 18224–18231 (2014).
27. Y. Ding, C. Peucheret, H. Ou, and K. Yvind, "Fully etched apodized grating coupler on the soi platform with- 0.58 db coupling efficiency," *Opt. Lett.* **39**(18), 5348–5350 (2014).
28. D. Benedikovic, P. Cheben, J. H. Schmid, D.-X. Xu, B. Lamontagne, S. Wang, J. Lapointe, R. Halir, A. Ortega-Moñux, S. Janz, and M. Dado, "Subwavelength index engineered surface grating coupler with sub-decibel efficiency for 220-nm silicon-on-insulator waveguides," *Opt. Express* **23**(17), 22628–22635 (2015).
29. J. Robinson and Y. Rahmat-Samii, "Particle swarm optimization in electromagnetics," *IEEE Trans. Antennas Propag.* **52**(2), 397–407 (2004).
30. C. W. Haggans, R. K. Kostuk, and L. Li, "Effective-medium theory of zeroth-order lamellar gratings in conical mountings," *J. Opt. Soc. Am. A* **10**(10), 2217–2225 (1993).
31. F. Van Laere, T. Claes, J. Schrauwen, S. Scheerlinck, W. Bogaerts, D. Taillaert, L. O'Faolain, D. Van Thourhout, and R. Baets, "Compact focusing grating couplers for silicon-on-insulator integrated circuits," *IEEE Photonics Technol. Lett.* **19**(23), 1919–1921 (2007).
32. D. Vermeulen, Y. De Koninck, Y. Li, E. Lambert, W. Bogaerts, R. Baets, and G. Roelkens, "Reflectionless grating couplers for silicon-on-insulator photonic integrated circuits," *Opt. Express* **20**(20), 22278–22283 (2012).
33. A. E.-J. Lim, J. Song, Q. Fang, C. Li, X. Tu, N. Duan, K. K. Chen, R. P.-C. Tern, and T.-Y. Liow, "Review of silicon photonics foundry efforts," *IEEE J. Sel. Top. Quantum Electron.* **20**(4), 405–416 (2014).

## 1. Introduction

Silicon photonics, based on the silicon-on-insulator (SOI) platform, provides an unprecedented opportunity to make highly integrated photonic circuits with sub-micron silicon-wire waveguides. However, the small feature sizes of waveguides raise the problem of large mode mismatch when coupling light from optical fibers to the sub-micron silicon waveguide cores. Edge coupling [1, 2] and surface coupling [3–14] are two popular approaches to address the mode mismatch issue. Surface coupling using grating couplers provides the flexibility to be placed anywhere on the chip, which enables better architectural design. Grating couplers also enable chip or wafer-scale automated measurement, without the need to dice the wafer. However, the disadvantages of using grating couplers are their polarization dependency and narrow operating bandwidth. Most grating

couplers that have been demonstrated so far are operating at C-band (around 1.55 μm) [3–7]. However, the short-reach data communications are often operating at O-band (around 1.31 μm) to benefit from the zero-dispersion feature of standard single-mode optical fibers. There are only a few works that are targeting at grating coupler designs for O-band application [4, 8–14], and all of them are devoted to improve the coupling efficiency of grating couplers. However, the operating bandwidth of a grating coupler is as important as the coupling efficiency, especially for wavelength division multiplexing (WDM) systems with large channel spacing. Sub-wavelength gratings (SWGs), with the flexibility to engineer both the index profile and the dispersion property, have been used to improve the performance of various integrated photonic components [15], such as wavelength multiplexers [16], low loss waveguide crossings [17], nanophotonic beam splitter [18], enhanced ring resonator biosensor [19], etc. SWGs have also been used to improve the coupling efficiency and the operating bandwidth of grating couplers [20–28]. However, it is more challenging to design grating couplers, especially sub-wavelength grating couplers (SWG Cs), for O-band applications because smaller feature sizes are required if a scaling approach is used [12].

In this paper, we demonstrate two SWGCs both operating at O-band: one targeting at high coupling efficiency and the other targeting at broad operating bandwidth. In the following of the paper, we will call them high-efficiency SWGC and broadband SWGC. The fabrication of our SWGC only requires a single etching step, which provides an efficient and economical solution for rapid prototyping. One-dimensional SWGs have been used in our SWGCs, which have the following advantages as compared to two-dimensional SWG structures that have been used in most previous works [23–28]. From the fabrication perspective, the one-dimensional SWGs are less challenging to fabricate because they benefit from higher exposure contrasts [20] and shorter fabrication times, resulting in high fabrication accuracy and lower fabrication cost. From the design perspective, due to the use of one dimensional SWGs, the design parameters of our SWGCs can be optimized using 2D simulations, which dramatically reduced the simulation time and requirement for computational memory.

## 2. Design and Simulations

Our SWGCs are designed for SOI wafers with a 220 nm silicon layer and a 2 μm buried oxide (BOX) layer. The schematic of the high-efficiency SWGC is shown in Fig. 1(a), which consist of alternating high and low index regions with lengths of  $\Lambda_{hH}$  and  $\Lambda_{hL}$ , respectively. The high index regions are made of silicon and the low index regions are made of SWGs with associated gaps filled with cladding material, which is silicon oxide in our case. The SWGs are small enough which operate in the subwavelength regime [15]. Therefore, the diffraction effects are suppressed and the low index regions can be treated as homogeneous material with an averaged index. The length of the SWGs in the low index regions is denoted by  $l_{\text{sub}}$ . The period of the high-efficiency SWGC is denoted by  $\Lambda_h$ , where  $\Lambda_h = \Lambda_{hH} + \Lambda_{hL}$ . The fill factor of the high-efficiency SWGC,  $f_{f_h}$ , is defined as the ratio of  $\Lambda_{hH}$  to  $\Lambda_h$ .

The schematic of the broadband SWGC is shown in Fig. 1(b), which also consists of alternating high and low index regions with lengths of  $\Lambda_{bH}$  and  $\Lambda_{bL}$ , respectively. Multiple SWGs are used in both the high and low index regions of the broadband SWGC. The lengths of the SWGs in the high and low index regions are denoted by  $l_H$  and  $l_L$ , respectively. Fill factor of the broadband SWGC,  $f_{f_b}$ , is defined as the ratio of  $\Lambda_{bH}$  to  $\Lambda_b$ . The numbers of gratings in each high and low index region are  $N_H$  and  $N_L$ , respectively. The fill factors of the high and low index regions, denoted by  $f_{fH}$  and  $f_{fL}$ , are defined as  $N_H * l_H / \Lambda_H$  and  $N_L * l_L / \Lambda_L$ , respectively.

The finite-difference time-domain (FDTD) method was used to optimize the design parameters of our SWGCs. We used FDTD Solutions, an FDTD-method Maxwell equation solver from Lumerical Solutions, Inc. for the optimization of our SWGCs. Due to the fact that we used one-dimensional SWGs, 2D FDTD simulations can be used to optimize various design parameters

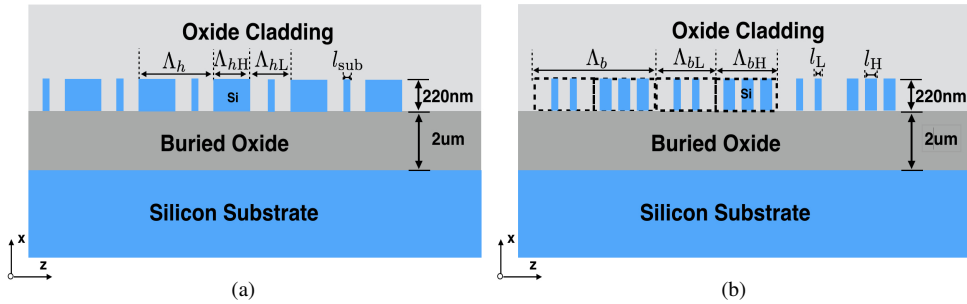


Fig. 1. Schematics of the cross-sections of (a) the high-efficiency O-band SWGC, and (b) the broadband O-band SWGC.

of our SWGCs, which dramatically reduced the simulation time. The high-efficiency SWGC was optimized in two steps, where the schematics of our simulations are shown in Fig. 2. In the first step, we optimized three design parameters,  $\Lambda_h$ ,  $f f_h$ , and  $l_{\text{sub}}$  of the high-efficiency SWGC. As shown in Fig. 2(a), the light was launched within the waveguide and then diffracted by the grating. A power monitor was positioned on top of the grating to measure the upward power, and the incident angle,  $\theta_h$ , of the SWGC can be calculated from the far field diffraction angle at the operating wavelength,  $\lambda$ , which is 1310 nm in our case. The goal in this step is to achieve the highest directionality, which defines as the ratio of the upward power to the input power. Particle swarm algorithm [29] has been used with FDTD simulations to obtain the highest directionality. Uniform gratings have been used in our design, which has an exponentially decaying power. Therefore, there is a mode mismatch between the out-coupled mode from the grating and fiber mode, which has an Gaussian profile. Further improvement can be made by applying apodization to the SWGC to achieve better mode match. In our case, the optimized high-efficiency SWGC in the first step has a directionality of 0.61. In the second step, as shown in Fig. 2(b), the input was launched from the fiber with the incident angle calculated from the first step. A mode expansion monitor was positioned in the waveguide to calculate the coupled power into the fundamental transverse electric (TE) mode. The position of the fiber was also optimized to achieve the highest coupling efficiency for our SWGC. The optimized design parameters of our high-efficiency SWGC are summarized in Table 1.

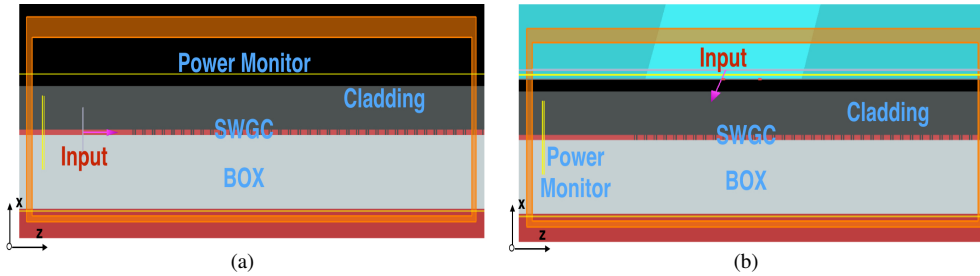


Fig. 2. Schematics of the simulations for the high-efficiency SWGC (a) with input from the waveguide, and (b) with input from the fiber.

Table 1. Design Parameters for the Optimized O-band High-Efficiency SWGC

PI.	$\lambda$ (nm)	$\Lambda_h$ (nm)	$f f_h$	$l_{\text{sub}}$ (nm)	$\theta_h$ ( $^{\circ}$ )
TE	1310	630	0.62	80	34

The optimization of our broadband SWGC follows a four-step process. The bandwidth of a grating coupler can be expressed as [22]:

$$\Delta\lambda_{3dB} = \Delta\theta_{3dB} \cdot 2 \left| \frac{-n_c \cdot \cos(\theta) \cdot \lambda}{n_g - n_c \cdot \sin(\theta)} \right| \quad (1)$$

where  $n_c$  is the refractive index of the cladding,  $n_g$  is the group index of the grating, and  $\theta$  is the incident angle.  $\Delta\theta_{3dB}$  is a constant that depends solely on the fiber parameters. Equation (1) shows that the bandwidth of a grating coupler can be increased by reducing  $n_g$  of the grating coupler. For a given  $n_g$ , the optimal incident angle, that gives the largest bandwidth, can be calculated for a specific  $\lambda$ . In the first step, we choose the incident angle,  $\theta_b$ , to be  $30^\circ$  based on an estimated  $n_g$ . In order to get the estimated  $n_g$ , we need to first estimate the effective index,  $n_{eff}$ , of the grating. The  $n_{eff}$  of the optical mode in a 220 nm silicon slab at 1310 nm is about 3, and the  $n_{eff}$  of the optical mode in silicon oxide is about 1.45. Assuming the overall fill factor of the grating is 0.5, then the averaged  $n_{eff}$  of the grating is about 2.2. Next, we used an eigenmode solver to calculate the equivalent refractive index of the grating, which is 2.75 in our case. Then, we calculate  $n_g$  with the equivalent refractive index, which give us  $n_g \approx 2.8$ . By applying the  $n_g$  into Equation (1), we can obtain the optimal incident angle that gives us the largest bandwidth, which is  $30^\circ$  in our case. The material dispersion was not included in the calculation due to the fact that we used a constant refractive index for the estimation. In the second step, the SWGC is simulated as alternating high and low index regions, as shown in Fig. 3(a), with refractive indices of  $n_H$  and  $n_L$  for the high and low index regions, respectively. A figure of merit (FOM), defined as the product of the 3-dB bandwidth and the coupling efficiency, is used to evaluate the performance of the SWGC. In this step, we optimize  $\Lambda_b$ ,  $f f_b$ ,  $n_H$  and  $n_L$  using 2D FDTD simulations with PSA to achieve the highest FOM. The optimized  $n_H$  and  $n_L$  we obtained in this step are 2.7 and 2, respectively. In the third step, we optimize  $f f_H$  and  $f f_L$ . In this step, the initial values for  $f f_H$  and  $f f_L$  are calculated using zeroth-order effective medium theory (EMT) [30], and then optimized using the 2D FDTD simulations with PSA to achieve the highest FOM. Finally, we optimize  $N_H$  and  $N_L$ , as shown in Fig. 3(b). It should be kept in mind that the dimensions of the SWGs have both a lower limit, which comes from the fabrication limitations, and an upper limit, which is determined by EMT. The dimensions of the SWGs should be small enough to allow EMT to work and large enough to be fabricated. The optimized design parameters of our broadband SWGC are summarized in Table 2.

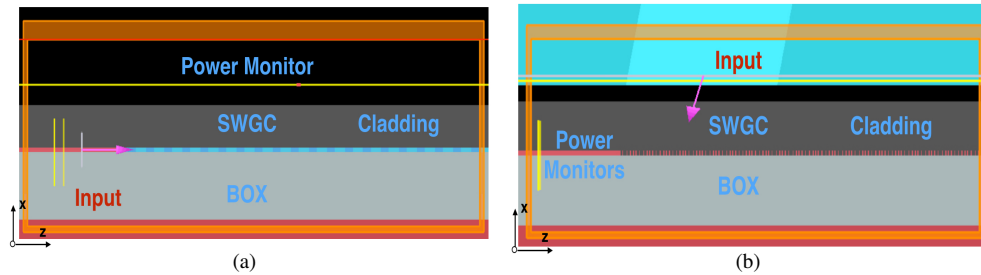


Fig. 3. Schematics of the simulations for the broadband SWGC (a) with virtual refractive indices of  $n_H$  and  $n_L$ , and (b) with actual SWGs.

Table 2. Design Parameters for the Optimized O-band Broadband SWGC

PI.	$\lambda$ (nm)	$\Lambda_b$ (nm)	$f f_b$	$f f_H$	$f f_L$	$N_H$	$N_L$	$\theta_b$ ( $^\circ$ )
TE	1310	924	0.5	0.46	0.17	3	2	30

So far we have addressed the SWGCs as a two-dimensional structure and assumed that the grating is extended in the lateral (Y) direction. However, long adiabatic tapers are required to couple the light from the grating into the sub-micron waveguides, with typical length over a few hundred microns, which are not space efficient and consumes valuable on-chip real estate. Focusing grating have been demonstrated and widely used as an alternative to achieve efficient mode size conversion [31]. In addition, by using the focusing gratings, the back reflection from the grating can be reduced significantly by offsetting the foci of the diffraction wave and reflection wave from the grating [32]. Focusing gratings have been used in our SWGCs to reduce the design footprints and to suppress the back reflection of our SWGCs. The dimensions of our SWGCs are smaller than  $45\text{ }\mu\text{m} \times 24\text{ }\mu\text{m}$ . Three-dimensional (3D) FDTD simulations for the full structures of our SWGCs have been done to confirm the optimized designs we obtained using 2D simulations. For comparison purposes, both the 2D and 3D simulation results for our high-efficiency and broadband SWGCs are shown in Fig. 4. We can see that our 3D simulations agree well with the 2D simulations except that the coupling efficiencies are slightly lower, which is due to the fact that the lateral dimension of gratings in the 3D simulations are not infinite as they are in the 2D simulations. Our high-efficiency SWGC has a simulated peak coupling efficiency of  $-2.9\text{ dB}$  with a 3-dB bandwidth of 41 nm (1-dB bandwidth of 24 nm), and the broadband SWGC has a simulated peak coupling efficiency of  $-3.3\text{ dB}$  with a 3-dB bandwidth of 75 nm (1-dB bandwidth of 46 nm).

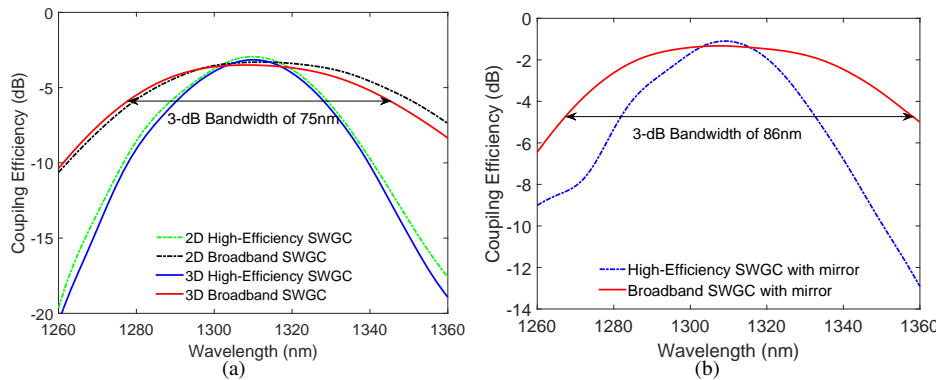


Fig. 4. (a) 2D and 3D simulation results for the high-efficiency and broadband SWGCs with 220 nm silicon layer, and (b) 2D simulation results for the high-efficiency and broadband SWGCs with 220 nm silicon layer and bottom mirror.

The major loss of our SWGCs comes from the penetration loss into the silicon substrate. In our case, the penetration loss for the high-efficiency and broadband SWGCs are  $1.6\text{ dB}$  and  $2.4\text{ dB}$ , respectively. In addition, the thicknesses of the top silicon layer and the BOX layer are not optimal to achieve high coupling efficiency for our design. We designed our SWGCs for SOI wafers with 220 nm silicon layer due to the availability of SOI wafers we have for fabrication and the popularity of such wafer that are offered by Multi Project Wafer (MPW) foundry services [33]. Bottom mirrors have been used to further improve the coupling efficiencies of grating couplers by reducing the penetration loss [6, 27, 28]. We simulated our SWGCs with bottom mirrors by placing a metal layer at the interface of the BOX and the silicon substrate. The results are shown in Fig. 4(b). The coupling efficiencies of the high-efficiency and broadband SWGCs can be increased to  $-1\text{ dB}$  and  $-1.3\text{ dB}$ , respectively; the 3-dB bandwidths are also improved to 46 nm and 86 nm, respectively. It should be noted that the BOX thickness is critical as it determines the inference between the beam reflected at the BOX-substrate interface and the upward radiated beam. The coupling efficiency of the SWGC varies periodically as the thickness of the BOX

varies, and the optimal values of the BOX thickness are those positions where constructive interference occurs between the beam reflected at the BOX-substrate interface and the upward diffracted beam.

### 3. Fabrication and Measurement

Test structures of our SWGCs, consisting of an input SWGC and an output SWGC with a spacing of 127  $\mu\text{m}$ , connected by a strip waveguide, were fabricated using electron beam lithography at Applied Nanotools Inc. Scanning electron microscope (SEM) images of the fabricated SWGCs are shown in Fig. 5. A fiber array based custom-built test setup with a Yenista TUNICS T100S-HP O-band tunable laser and a CT400 passive optical component tester were used to characterize the fabricated devices. The wavelength was swept from 1260 nm to 1360 nm in 10 pm steps.

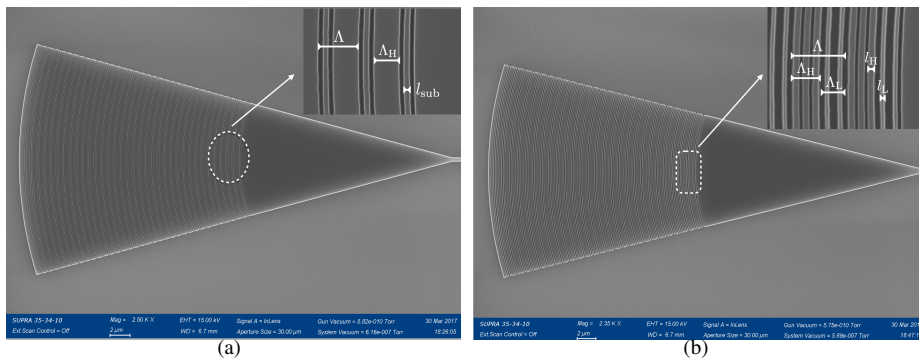


Fig. 5. SEM images of the fabricated (a) high-efficiency SWGC, and (b) broadband SWGC.

The measured spectra for the high-efficiency and broadband SWGCs are shown in Fig. 6. The high-efficiency SWGC has a measured peak coupling efficiency of  $-3.8$  dB with a 3-dB bandwidth of 41 nm (1-dB bandwidth of 21 nm). The broadband SWGC has a measured peak coupling efficiency of  $-4.3$  dB with a 3-dB bandwidth of 71 nm (1-dB bandwidth of 38 nm). The measured 3-dB bandwidth of our broadband SWGC is the largest value that has been reported to the best of our knowledge. The insertion losses from the CT-400, the polarization controller, and the fiber patchcords connecting them have been calibrated out, while the insertion loss from the fiber array is included in the results shown in Fig. 6. The measured coupling efficiencies and bandwidths of our SWGCs agrees well with the simulation results shown in Fig. 4(a) except for the small mismatch in coupling efficiencies, which we think resulted from the uncalibrated insertion loss from the fiber array and connectors we used in our measurement and the unavoidable fabrication imperfections. Small oscillation ripples can be observed in the measured spectra of the SWGCs, which resulted from the back reflections of the SWGCs. The extinction ratios (ERs) of the oscillation ripples for both the high-efficiency and broadband SWGCs are about 0.2 dB in the wavelength range from 1280 nm to 1360 nm, which indicates back reflections from the SWGCs are around  $-20$  dB. The back reflections from the SWGCs increase as the wavelength decreases, thus stronger oscillation ripples are observed in the shorter wavelength regions of the measured spectrum. The ERs of the oscillation ripples are about 0.5 dB in the wavelength range from 1260 nm to 1280 nm, which indicates back reflections from the SWGCs are around  $-15.5$  dB.

In order to test the robustness and repeatability of our SWGCs, multiple copies of the test structures with the same design parameters are fabricated on the same chip. The peak coupling efficiencies and the 3-dB bandwidths of the measured SWGCs are extracted and shown in Figs. 7(a) and 7(b), respectively. The measured peak coupling efficiencies of the high-efficiency and broadband SWGCs vary from  $-4.3$  dB to  $-3.8$  dB and from  $-4.5$  dB to  $-4.2$  dB, respectively,

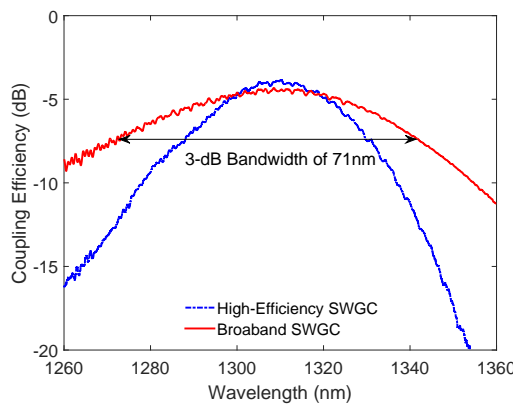


Fig. 6. Comparison of the measured coupling efficiencies as a function of wavelength for the high-efficiency and broadband SWGCs.

while the 3-dB bandwidths vary from 41 nm to 45 nm and from 65 nm to 71 nm, respectively. From Fig. 7, we can see that performance of our SWGCs are quite stable, with peak coupling efficiency variation no more than 0.5 dB and 3-dB bandwidth variation no more than 6 nm. We noted that some of the measured 3-dB bandwidths for the high-efficiency SWGCs are even better than the simulated value, while the measured 3-dB bandwidths for the broadband SWGCs are slightly lower than the simulated value, which we think resulted from the fabrication imperfections in the oxide cladding thickness. The bandwidths of the SWGCs changes sinusoidally as the cladding thickness changes. However, the optimal thickness values for the high-efficiency and broadband SWGCs are different. We chose one of the optimal thickness values for the broadband SWGC as the target oxide cladding thickness for the fabrication, which is not optimal for the high-efficiency SWGC. Due to the fabrication imperfections or the non-uniformity of the cladding thickness across the chip, the actual cladding thickness may offset from the optimal value for the broadband SWGC and ended up as a better value for the high-efficiency SWGC.

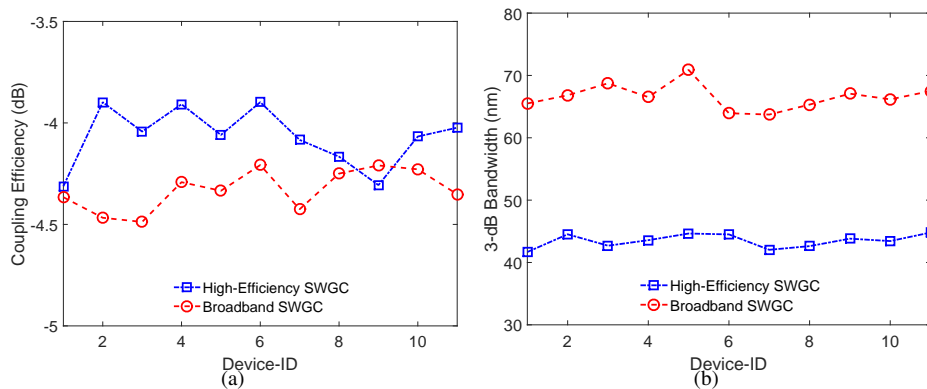


Fig. 7. (a) Peak coupling efficiencies, and (b) 3-dB bandwidths of the high-efficiency and broadband SWGCs extracted from multiple test structures.

The performance sensitivity to various design parameters of our SWGCs have been investigated. For the high-efficiency SWGC, we applied variations to  $\Lambda_{hH}$  and  $l_{\text{sub}}$ . For the broadband SWGC, we only applied variations to  $l_H$  because  $l_L$  is close to the fabrication limitation. Therefore, no variations have been applied to it. Test structures of high-efficiency SWGCs with  $\Lambda_{hH}$  and  $l_{\text{sub}}$  varied within  $\pm 15$  nm and broadband SWGCs with  $l_H$  varied within  $\pm 12$  nm have been

fabricated. According to the Bragg condition, the central operating wavelength of the grating coupler is proportional to the effective index of the grating. Thus, as we vary  $\Lambda_{hH}$  and  $l_{\text{sub}}$  for the high-efficiency SWGC and  $l_H$  for the broadband SWGC, the central operating wavelengths of our SWGCs vary accordingly. In addition, the change in the effective index of the grating also affects the interference behaviour of the grating, which then affects the peak coupling efficiency of a grating coupler. The measured central wavelength change,  $\Delta\lambda$ , and peak coupling efficiencies of our SWGCs as a function of the grating dimension change,  $\Delta W$ , are shown in Fig. 8. For the high-efficiency SWGC, the central operating wavelength varies at a similar rate as we change the  $\Lambda_{hH}$  and  $l_{\text{sub}}$ , respectively. However, a much larger loss penalty is observed as we vary  $l_{\text{sub}}$ . This is the case because both the effective index of the grating and the index contrast of the grating have been changed as we change  $l_{\text{sub}}$  of the high-efficiency SWGC, while only the effective index of the grating is changed as we change  $\Lambda_{hH}$ . Due to the fact that both the high and low index regions of our broadband SWGCs are made of SWGs, the change in  $l_H$  has a larger impact on both the effective index and index contrast of the grating. Therefore, the central operating wavelength and peak coupling efficiency of our broadband SWGC are more sensitive than the high-efficiency SWGC.

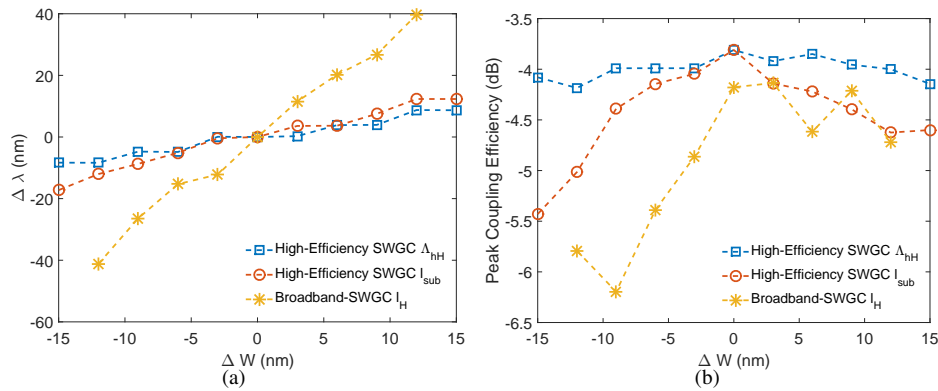


Fig. 8. (a) Central operating wavelength change as a function of grating dimension change, and (b) peak coupling efficiency as a function of grating dimension change.

#### 4. Conclusion

In conclusion, we demonstrated two SWGCs operating at O-band. The high-efficiency SWGC has a measured peak coupling efficiency of  $-3.8$  dB with a 3-dB bandwidth of 41 nm and the broadband SWGC has a measured peak coupling efficiency of  $-4.3$  dB with a 3-dB bandwidth of 71 nm. The measured 3-dB bandwidth of our broadband SWGC is the largest value that has been reported so far. Back reflections from our SWGCs have been well suppressed to be below  $-15$  dB over the entire O-band. The fabrication of our SWGC only requires a single etching step, which provides an efficient and economical solution for rapid prototyping. One-dimensional SWGs have been used in our SWGCs, thus 2D simulations can be used to optimize various design parameters, dramatically reducing the simulation time. Focusing gratings have been used to reduce the design footprints and the dimensions of our SWGCs are smaller than  $45 \mu\text{m} \times 24 \mu\text{m}$ . The robustness, repeatability and sensitivity of our SWGCs have been investigated.

#### Acknowledgment

We would like to acknowledge CMC Microsystems for providing access to simulation and CAD tools.